Locating and quantifying CH₄ sources within a wastewater treatment plant based on mobile measurements

Junyue Yang[1], Zhengning Xu[1], Zheng Xia[4,5], Xiangyu Pei[1], Yunye Yang[1], Botian Qiu[2,3], Shuang Zhao[2,3], Yuzhong Zhang[2,3*], Zhibin Wang[1,6*]

[1]Zhejiang Provincial Key Laboratory of Organic Pollution Process and Control, MOE Key Laboratory of Environment Remediation and Ecological Health, College of Environmental and Resource Sciences, Zhejiang University, Hangzhou 310058, China

[2]Key Laboratory of Coastal Environment and Resources of Zhejiang Province, School of Engineering, Westlake University, Hangzhou 310030, China

[3]Institute of Advanced Technology, Westlake Institute for Advanced Study, Hangzhou 310024, China

[4]Ecological and Environmental Monitoring Center of Zhejiang Province, Hangzhou 310012, China

[5]Zhejiang Key Laboratory of modern Ecological and Environmental Monitoring, Hangzhou 310012, China

[6]ZJU-Hangzhou Global Scientific and Technological Innovation Center, Zhejiang University, Hangzhou 311200, China

Correspondence to: Zhibin Wang (wangzhibin@zju.edu.cn) and Yuzhong Zhang (zhangyuzhong@westlake.edu.cn)

Abstract. Wastewater treatment plants (WWTPs) are substantial contributors to greenhouse gas (GHG) emissions because of the high production of methane (CH_4) and nitrous oxide (N_2O). A typical WWTP complex contains multiple functional areas that are potential sources for GHG emissions. Accurately quantifying GHG emissions from

these sources is challenging due to the inaccuracy of activity data, the ambiguity of emission sources, and the absence of monitoring standards. Locating and quantifying WWTPs emission sources using measurement-based GHG emission quantification method is crucial for evaluating and improving traditional emission inventories. In this study, CH_4 mobile measurements were conducted within a WWTP complex in the summer and winter of 2023. We utilized a multi-source Gaussian plume model combined with the genetic algorithm inversion framework, designed to locate major sources within the plant and quantify the corresponding CH_4 emission fluxes. We identified 13 main sources in the plant and estimated plant-scale CH_4 emission fluxes of 68.78 ± 17.40 kg h^{-1} (603.33 ± 152.66 t a^{-1}) for the summer and 47.76 ± 21.39 kg h^{-1} (418.95 ± 187.59 t a^{-1}) for the winter. The predominant sources of CH_4 emissions were the screen and primary clarifier, contributing 55 % and 67 % to the total emissions in summer and winter, respectively. The comparison revealed that summer CH_4 emissions were 2.8 times higher than inventory estimates, while winter emissions were twice the inventory values. This study demonstrated that mobile measurements, combined with the multi-source Gaussian plume inversion framework, are a powerful tool to locate and quantify GHG sources in a complex site, with the potential for further refinement to accommodate different types of factories and gas species.

1 Introduction

Methane (CH_4) is the second-largest contributor to climate change, with the global warming potential 27.9 times that of carbon dioxide (CO_2). Reducing CH_4 emissions is essential for mitigating climate change and progressively achieving the global target of limiting warming to 1.5 °C (IPCC, 2023). WMO Global Atmospheric Watch network indicated that the global annual average concentration of CH_4 in 2022 was 1923 ± 2 ppb, representing a 264 % increase from pre-industrial levels (WMO, 2023). The International Energy Agency (IEA) 2024 Global Methane Tracker report suggests that

global CH$_4$ emissions reached 580 Mt in 2023, with anthropogenic CH$_4$ emissions accounting for 60 %. The complexity of CH$_4$ emission processes, lack of monitoring systems, and limitations of emission estimation models present challenges in accurately estimating anthropogenic CH$_4$ emissions.

The quantification of CH$_4$ emission fluxes is typically achieved through a bottom-up inventory method. However, due to the difficulties in obtaining activity data used for actual emission factors, and specific information on different emission sources, there is considerable uncertainty in the assessing of the emission inventory method (Lin et al., 2021). In contrast, a top-down method that estimates CH$_4$ emissions by monitoring atmospheric concentration has been increasingly applied in recent years (Sun et al., 2019; Cusworth et al., 2024; Han et al., 2024; Maazallahi et al., 2023; Riddick et al., 2017). The monitoring technology mainly includes satellite (Zhang et al., 2021; Liang et al., 2023; Jacob et al., 2022) and airborne (Allen et al., 2019; Abeywickrama et al., 2023; Cui et al., 2017) remote sensing, as well as ground-based monitoring such as vehicle-based mobile monitoring (Albertson et al., 2016; Al-Shalan et al., 2022; Caulton et al., 2018), station monitoring (Dietrich et al., 2021; Hase et al., 2015; Heerah et al.,2021) and tower monitoring (Richardson et al., 2017; Balashov et al., 2020). Emission flux inversion methods also include isotope tracer method (Jackson et al., 2014; Zimnoch et al., 2018), cross-sectional flux method (Luther et al., 2019; Makarova et al., 2021), and atmospheric diffusion model inversion method (Kumar et al., 2021; Yacovitch et al., 2015). Atmospheric transport models with varied degrees of complexity, including Gaussian diffusion models (Stadler et al., 2021), Lagrangian models (Mckain et al., 2015), and Eulerian models (Bergamaschi et al., 2018), are used in the inversion to relate GHG concentrations with emissions. Optimization methods, such as Bayesian optimization (Karion et al., 2019) and linear regression models (Kumar et al., 2021), are applied to achieve accurate inversion results. Furthermore, some studies incorporate carbon isotope observations to better attribute the contribution of different CH$_4$ emission sources (Maazallahi et al., 2020). Numerous studies use

satellite remote sensing, unmanned aerial vehicle (UAV) monitoring, and vehicle-based mobile monitoring techniques to measure CH_4 emissions (Sun et al.,2023). However, satellite spatiotemporal resolution is limited and UAVs have short endurance, making vehicle-based mobile monitoring a better choice for measuring CH_4 emissions. Vehicle-based mobile monitoring can perform continuous real-time monitoring and precise identification of emission sources, and hence have been applied to urban (von Fischer et al., 2017; Defratyka et al., 2021) and plant-scale (Zhao et al., 2021; Jin et al.,2010) monitoring of GHG concentrations and emission fluxes. Vogel et al. (2024) used high-precision fast-response GHG analyzers to investigate CH_4 leaks in 12 cities across eight countries. Chen et al. (2020) utilized the multiple-Gaussian-plume model for mobile measurements of CH_4 emissions during the Munich Oktoberfest. Shi et al. (2023) conducted mobile measurements with vehicle-based monitoring system at chemical, coal washing, and waste incineration plants in two cities and one industrial park in China.

As a significant source of GHG emissions, wastewater treatment plants (WWTPs) generate substantial amounts of CH_4, N_2O, and CO_2 during the collection, treatment, and discharge of sewage and sludge, contributing 3 % of the global total GHG emissions (Bai et al., 2022). The estimation of CH_4 emission fluxes from WWTPs has increasingly attracted widespread attention. Li et al. (2024) developed a plant-level and technology-based CH_4 emission inventory for municipal WWTPs in China, estimating the CH_4 emissions for 2020 to be 150.6 Gg. Delre et al. (2017) measured the CH_4 concentrations downwind of five WWTPs in Scandinavia using tracer gas dispersion, which obtained a range of CH_4 emission fluxes from 1.1 ± 0.1 to 18.1 ± 6.3 kg h^{-1}. Moore et al. (2023) employed CH_4 mobile measurements from 63 WWTPs in the United States, pointing to a significant underestimation in the CH_4 emission inventories. However, most studies lack comparisons between measured and simulated concentrations, resulting in significant uncertainty in the results. We present a mobile measurement investigation of a WWTP in Hangzhou 2023. To analyze the mobile data,

we construct a multi-source Gaussian plume model combined with the genetic algorithm inversion framework, which assists us to locate and quantify CH_4 emission sources, based on the concentration distribution measured within the WWTP. Additionally, we compare CH_4 emission fluxes from the measurements with the bottom-up estimates of emission inventories. A sensitivity analysis is performed to elucidate the discrepancies arising from variations in emission source locations. Our results provide insight into formulating and evaluating emission reduction measures for WWTPs.

2 Instruments and methods

2.1 Site selection

The monitoring site was chosen at a WWTP in Hangzhou, a megacity in East China. This WWTP is a large-scale plant located in Hangzhou, processing up to 1.5 million tons of domestic wastewater daily. The chosen WWTP processes encompass mechanical treatment, biological treatment, sedimentation, advanced treatment, disinfection, and sludge treatment. As illustrated in Fig. 1, we divide the WWTP into 14 functional areas according to treatment processes. Areas associated with primary treatment were labeled as coarse screens and primary sedimentation tanks, while those linked to secondary treatment were indicated as aeration tanks and secondary sedimentation tanks. We performed one monitoring experiment per day, with each experiment entailing 1-2 rounds of mobile measurements along external roads and internal functional areas roads. Additionally, we conducted repeated mobile measurements and fixed measurements on roads with high concentrations to calculate average concentration data. Over 10 days of experiments from June to December 2023, we obtain 8 days of complete monitoring data, including 3 days in summer and 5 days in winter. On the other two experimental days, internal facility maintenance restricted

135 access to certain roads, resulting in incomplete monitoring data.

136

137 **Figure 1.** Distribution of functional areas of the WWTP. The yellow mark represents

138 the simulated location of the line source. Solid lines show the roads measured by the

139 mobile vehicle. Map data are from ESRI.

2.2 Instrumentation

141   The monitoring instruments consisted of a vehicle-mounted Cavity Ring-Down

142 Spectrometer (CRDS) monitoring system (Zhao et al., 2024) and a portable

143 meteorological station. The vehicle-mounted CRDS system was anchored by the CRDS

144 analyzer (Picarro G2201-i, Picarro 2010), accompanied by GPS and meteorological

145 instruments. The volume fraction of CH_4 is measured with an accuracy of 5 ppb $\pm$

146 0.05 %. CRDS measurements have the advantages of strong interference resistance,

147 high sensitivity and accuracy, making them widely employed in research focused on

148 monitoring GHG emissions (Rella et al., 2015; Lopez et al., 2017).

149   In this study, the CRDS analyzer was placed inside the monitoring vehicle to measure

150 CH_4 concentrations in the WWTP. The sampling probe was placed near the roof along

151 the window of the car to avoid interference from vehicle exhaust due to the low position.

152 The mobile meteorological instrument was placed on the roof of the vehicle to gather

meteorological data. In addition, the GPS unit was integrated to record the location of sampling points during the measurement period. Two portable meteorological stations (Hangzhou Pengpu Technology SWS-500) were positioned adjacent to the main entrance and atop the filter tank at the WWTP. Capable of measuring meteorological parameters (wind speed, direction, temperature, humidity, and atmospheric pressure).

2.3 Inventory accounting method

We used the methods suggested by the IPCC Guidelines for National Greenhouse Gas Inventories (2006) to calculate the amounts of CH_4 emissions from wastewater. The formula for calculating the amounts of CH_4 emissions from wastewater is described as:

$$E_{CH_4} = (TOW - S \cdot a) \cdot EF_{CH_4} - R_{CH_4} \tag{1}$$

Where E_{CH_4} denotes the direct CH_4 emissions from the wastewater treatment plant, tCH_4 a^{-1}. TOW is defined as the total organic pollutant load in the influent wastewater, $tCOD$ a^{-1}. S refers to the annual production total of dry sludge, t a^{-1}. The parameter a signifies the organic matter content in the dry sludge, $tCOD$ t^{-1}. EF_{CH_4} is the CH_4 emission factor, tCH_4 $tCOD^{-1}$. R_{CH_4} quantifies the annual recovery of CH_4 from anaerobic treatment processes, t a^{-1}.

Operational data of the WWTP examined in this study is derived from the Urban Drainage Statistical Yearbook, an annual publication of urban water supply and drainage systems in China. This data set includes details such as the water treatment volume, sludge production, and the concentrations of six pollutants (COD_{Cr}, BOD, SS, NH_3-N, TN, and TP) in both influent and effluent. The Total Organic Waste (TOW) is calculated by the amount of treated water and COD influent concentration of the WWTP provided in the yearbook, while the annual sludge production (S) is extracted directly from the yearbook. The organic matter content in dry sludge is estimated at an empirical 40 %, assuming a sludge moisture content of 75 %, leading to a value of 0.1 (Guo et al., 2019). EF_{CH_4} is selected based on the recommended value for Zhejiang

province, 0.0046 (Cai et al., 2015). Given the infrequency of anaerobic treatment in wastewater, R_{CH_4} is set to 0.

2.4 Inversion method

We developed an inversion framework for emission fluxes designed for plant-level applications. The framework used mobile measurements data, locations of emission sources, and initial emission estimates, alongside wind speed and direction data, as inputs to the multi-source Gaussian diffusion models. The preliminary localization of the emission sources was chiefly contingent upon the concentration distribution along the roads within the internal functional areas. Meanwhile, the initial emission estimates for each source were determined by integrating the concentration data from these areas with an improved empirical equation (Weller et al., 2019). Based on the comparison of measurement and model simulation results (Fig. S1), it is determined that the plant exhibits multiple point sources and line source diffusion patterns. Fig. S1 illustrates that the CH_4 concentration curve presents distinct peak distributions in point source diffusion patterns, while the CH_4 concentration distribution in line source diffusion patterns consistently maintains higher levels. We then used a genetic algorithm to iteratively optimize source emission fluxes and their locations. The inversion framework simulation dictated the placement of 12 main point sources throughout the WWTP, specifically within Aeration Tank ①②③④⑤, Primary Clarifier ③④⑤, Screen ①, Secondary Clarifier ①②, and the Sludge Treatment ② (Fig. 1). Within this study, a uniform line source was established, with the assumed location along the road between the Screen ① and the Primary Clarifier ① (Fig. 1 yellow mark). This assumption was grounded in the CH_4 concentration distribution observed within this road segment and was substantiated through model validation. The remaining emission flux inversion processes followed the same procedure as the point source simulation. Adjustments to the source locations within the model narrow the gap between simulated

206 and measured concentrations, thus enhancing the accuracy of inversion. This section

207 delineates each model incorporated into the inversion framework.

2.4.1 Empirical equation for estimating initial emissions

209 We used the improved empirical equation to estimate the initial emissions of

210 emission sources (von Fisher et al., 2017; Weller et al.,2019). This method was

211 primarily utilized for urban CH₄ leakage source emissions estimation (Defratyka et

212 al., 2021; Maazallahi et al., 2020). The empirical equation is as follows:

$$ln\left(M_{CH_4}\right) = -0.988 + 0.817 \times ln\ (CH_4\ emission\ rate) \qquad (2)$$

214 The M_{CH_4} is the maximum enhancement value of CH₄ concentration, ppm. The

215 *CH₄ emission rate* represents the CH₄ emission flux, L min^{-1}.

2.4.2 Multiple-point-source Gaussian plume model

217 We developed a multiple-point-source Gaussian plume model to relate CH₄

218 concentration enhancement to CH₄ emissions. This method approximates atmospheric

219 dispersion of CH₄ from an individual source as a Gaussian plume under uniform and

220 stable wind conditions (Nassar et al., 2017), which is usually good for describing

221 average atmospheric transport tens to hundreds of meters downwind the source, making

222 the Gaussian plume model a useful tool to study emissions from industrial and traffic

223 sources.

224 The mass concentration enhancement (*C,* mg m^{-3}) is computed as superposition of

225 Gaussian plumes from multiple point sources.

$$C(x,y,z) = \sum_{i=1}^{n} \frac{Q_i}{2\pi\bar{u}\sigma_{i,y}\sigma_{i,z}} exp\left(-\frac{(y-y_i)^2}{2\sigma_{i,y}^2}\right)\left\{exp\left[\frac{-(z-z_i)^2}{2\sigma_{i,z}^2}\right] + exp\left[\frac{-(z+z_i)^2}{2\sigma_{i,z}^2}\right]\right\} \qquad (3)$$

227 The variables *x*, *y*, and *z* denote the downwind, crosswind distances, and the height

228 above the ground from the source, m. Q_i signifies the emission rate from the i_{th} point

229 source, mg s^{-1}, for *i* = 1, 2, 3……N, where *N* represents the total count of point sources.

230 The average wind speed is indicated by $\bar{u}$, m s^{-1}. The x_i, y_i and z_i are represented

as the spatial position of the i_{th} point source, m. $\sigma_{i,y}$ and $\sigma_{i,Z}$ are the horizontal and vertical dispersion parameters of the i_{th} point source, respectively, which are given by the formula below:

$$\sigma_{i,y} = \gamma_1 \cdot (x - x_i)^{\alpha_1}, \; when \; x > x_i \tag{4}$$

$$\sigma_{i,z} = \gamma_2 \cdot (x - x_i)^{\alpha_2}, \; when \; x > x_i \tag{5}$$

The power functions, known as the Pasquill's curves, associates with the downwind distance x and the prevailing atmospheric stability (Briggs et al., 1973). Atmospheric stability is determined based on the Pasquill stability classes recommended in the Technical Principles and Methods for Formulating Local Air Pollution Emission Standards (GB3840-83). During the observation, the CH_4 concentrations were obtained through the vehicle-mounted CRDS monitoring system. The portable meteorological stations collected data on wind speed and direction, while GPS tracked the mobile paths to pinpoint emission source locations.

2.4.3 General Finite Line Source Model

Our analysis of measurement at WWTPs indicates that multiple-point-source Gaussian plume model is insufficient to capture the observed CH_4 concentrations. The entire road between the Screen ① and the Primary Clarifier ① shows high distribution of CH_4 concentrations. The contribution of a line source to CH_4 concentration is given by the General Finite Line Source Model (GFLSM) (Luhar et al., 1989; Venkatram et al., 2006), which represents the line source as an ensemble of point sources:

$$C = \frac{Q}{2\pi \bar{u} \sigma_y \sigma_z} \left\{ exp \left[\frac{-(z-H)^2}{2\sigma_Z{}^2} \right] + exp \left[\frac{-(z+H)^2}{2\sigma_Z{}^2} \right] \right\}$$

$$\cdot \left[erf \left(\frac{\sin\theta\left(\frac{L}{2}-y\right)-x\cos\theta}{\sqrt{2}\sigma_y} \right) + erf \left(\frac{\sin\theta\left(\frac{L}{2}+y\right)+x\cos\theta}{\sqrt{2}\sigma_y} \right) \right] \tag{6}$$

256   x, y, and z correspond to the downwind, crosswind distances, and the altitude above

257   ground level from the source, m. Q_i is the emission fluxes of the unit source, mg s^{-1}. $\bar{u}$

258   is the average wind speed, m s^{-1}. H_i is the effective emission height of the line source,

259   with the length of the line source represented by L, m. The angle between the line

260   source and the wind direction is given by θ. The horizontal and vertical dispersion

261   parameters are characterized by σ_y and σ_Z, respectively.

262 **2.4.4 Genetic algorithm**

263   Genetic algorithms, which mimic the evolutionary process of biological systems,

264   serve as optimization search algorithms. The algorithms encode practical problems into

265   binary genetic coding. Through the simulation of natural selection, crossover, and

266   mutation processes, these algorithms are in a constant state of evolution and iteration,

267   all in the pursuit of the optimal solution (Katoch et al., 2021). We deployed genetic

268   algorithms to enhance the source emission flux outcomes modeled by the Gaussian

269   plume model.

270   The process of inverting multi-source CH_4 emission fluxes utilizing genetic

271   algorithms involves a series of steps. Initially, the emission flux of each source is treated

272   as a gene, with binary-encoded gene sequences randomly assigned to a set number of

273   individuals within the predefined range of a priori emission fluxes. Subsequently, the

274   formulation of a fitness function is based on the defined optimization goals and

275   constraints. This function serves as a critical tool for assessing the relative merits of

276   each individual within the population. In this study, the objective of the optimization is

277   centered on minimizing the aggregate absolute discrepancy between the values

278   predicted by the model and those obtained from measurements. Ultimately, the

279   population is subjected to the processes of selection, crossover, and mutation.

280   Individuals with elevated fitness values, as determined by the fitness function, are

281   chosen for the generation of new individuals. Through an iterative process, the optimal

282   solution is refined, representing the emission fluxes for each source. Genetic algorithms

283 are distinguished by the parallel computation capabilities, the propensity for identifying

284 global optima, and the commendable stability and reliability (Harada et al., 2020).

285 **2.4.5 Uncertainty analysis**

286   To quantify the uncertainty in the inversion results, we have considered the

287 uncertainties associated with the input parameters of the inversion model, including

288 wind speed, wind direction, and instrument measurements. The uncertainty in the CH_4

289 emission fluxes (ε_t) is derived using the error propagation formula as follows:

290 $$\varepsilon_t = \sqrt{\varepsilon_s{}^2 + \varepsilon_d{}^2 + \varepsilon_m{}^2} \tag{7}$$

291   ε_s and ε_d denote the uncertainties in wind speed and direction, which are

292 determined by the standard deviation of the wind speed and direction measurements

293 from two fixed meteorological stations during the observation period. ε_m represents

294 the uncertainty in instrumental measurements. This uncertainty is derived from data

295 provided by the manufacturer Picarro, which indicates a concentration measurement

296 uncertainty of approximately 1 ppb for a 10-second integration time (Picarro 2010).

297

298 **3 Results and discussion**

299 **3.1 Concentration mapping**

300   The closed-path mobile measurements were conducted by vehicle-mounted CRDS

301 monitoring system along the external roads encircling the WWTP, with further

302 monitoring conducted along the internal roads. This strategy depicts the distribution of

303 CH_4 concentrations within an WWTP, allowing for identification of specific CH_4

304 emission sources. Based on 8 days of CH_4 monitoring experimental data, the CH_4

305 concentration range on the overall roads was determined to be 1.98-17.13 ppm. The

306 CH_4 concentration distribution indicated higher levels downwind, with the highest

307 concentrations consistently recorded at the Screen ① throughout mobile experiments.

308 Due to the consistency of concentration measurement methods, we chose 29th June

309 and 13th December as a typical example. Figure 2 illustrates measured CH_4

310 concentration enhancement distributions on 29th June (summer) and 13th December

311 (winter) 2023 (other days are shown in Figures S3-S8). The CH_4 concentration

312 enhancements depicted were calculated by subtracting the background concentrations

313 from the measured values, with the background determined as the mean of the bottom

314 10 % of the concentration data. Specifically, the background concentrations register at

315 1.98 ppm on 29th June and at a slightly elevated 2.11 ppm on 13th December. The

316 analysis indicates that the shallower boundary layer in winter causes CH_4 to accumulate

317 near the surface, resulting in a higher background concentration. Moreover, increased

318 concentrations are detected in the regions surrounding the Screen ①, Primary Clarifier

319 ④, and Aeration Tank ③ during these two days. The complete concentration maps ,

320 which include the internal roads, reveal that the experiment on 29th June exhibits

321 heightened concentrations at the Screen ①, Secondary Clarifier ②, and Primary

322 Clarifier ②④. The Screen ① exhibits the highest CH_4 concentration, with an

323 enhancement of 14.83 ppm. On 13th December, the concentration enhancements are

324 noted in proximity to the Secondary Clarifier ① and Primary Clarifier ②, with the

325 Primary Clarifier ② showing the highest CH_4 concentration at 4.79 ppm.

326 CH_4 concentrations in summer surpass those observed in winter, consistent with a

327 previous study on WWTPs (Masuda et al., 2015). The screen, primary clarifier and

328 aeration tank are identified as sources with notably higher concentrations. Analysis of

329 concentration distributions reveals that Screen ① shows a peak concentration reaching

330 14.83 ppm, which is 7.5 times the background concentration. The four primary

331 clarifiers record high concentrations between 4.79 and 10.88 ppm. The high value

332 measured by aeration tanks is mainly detected in Aeration Tank ③ at 4.60 ppm. The

333 screen in this study includes coarse and fine screens and a grit chamber, constituting

334 preliminary wastewater treatment to capture larger suspended solids and particulates.

335 The anaerobic environment of the sewer network promotes the production of CH_4 from

336 organic compounds in municipal wastewater. As this wastewater enters the WWTP, the

337 influent contains dissolved CH_4 that originated in the sewer network. During primary

338 treatment, wastewater is elevated through riser mains, facilitating the release of CH_4

339 into the atmosphere (Guisasola et al., 2008; Bao et al., 2016). Flow velocity, hydraulic

340 design and detention times in these facilities may affect CH_4 production and release

341 (Alshboul et al., 2016; Yin et al., 2024). The primary clarifier physically removes

342 suspended solids from wastewater through sedimentation, while organic matter

343 undergoes anaerobic microbial degradation to the substantial production of CH_4

344 (Masuda et al., 2017). In the aeration tank, operated under anaerobic and anoxic

345 conditions, complex organic compounds are converted to CH_4 by facultative and

346 anaerobic bacteria through biological processes (Yoshida et al.,2014). In contrast,

347 Kupper et al. (2018) identified sludge storage tanks as the primary source of CH_4

348 emissions in Swiss WWTPs, accounting for 70 % or more of the total emissions. Stadler

349 et al. (2022) monitored CH_4 concentrations inside and around wastewater treatment

350 facilities ranging from 2.04-32.78 ppm, with elevated CH_4 levels predominantly

351 measured near sludge treatment tank, the digesters and secondary clarifiers. CH_4

352 emissions from various WTTPs are affected by a range of factors, including specific

353 processes, pipeline design, and equipment aging, the mobile monitoring can better

354 reflect the actual emission distribution.
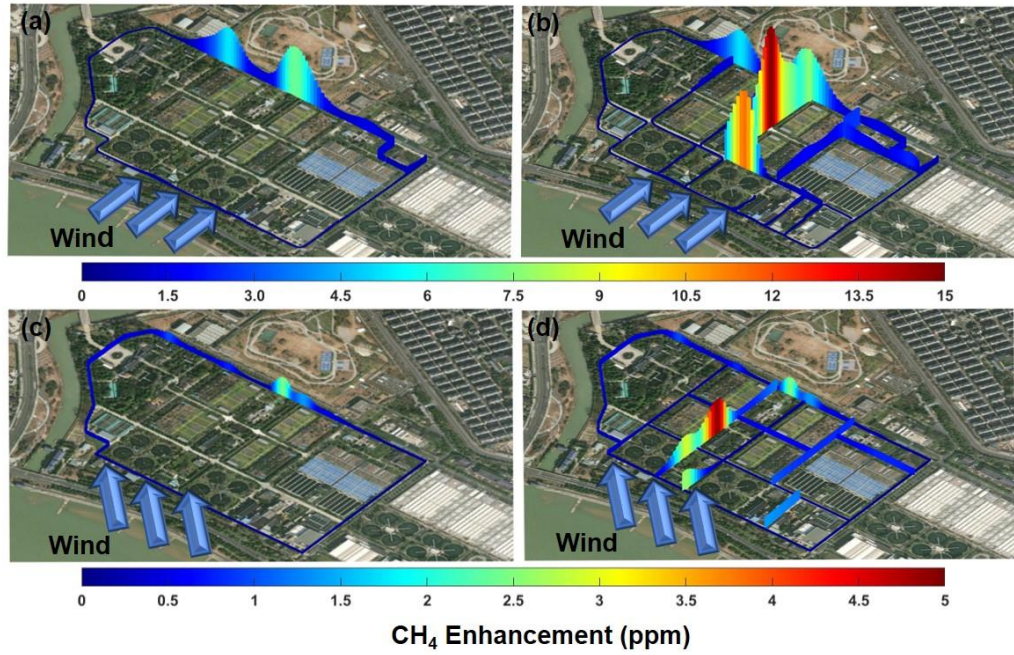
Figure 2. CH4 concentration maps in the WWTP. The concentration maps for the external roads for 29th June (a) and 13th December (c). The corresponding complete concentration maps that include the internal roads for 29th June (b) and 13th December (d). Map data are from ESRI.

3.2 Emission quantification

The mobile measured CH4 concentrations were employed in combination with the inversion framework to achieve the quantification of CH4 emissions and localization of the emission sources within the WWTP. Figures 3 and 4 show the locations of identified point sources and the comparison between measured and simulated concentration distribution. The experiment conducted on 29th June finds the Screen ① to be the most significant contributor to CH4 point source emissions at 18.26 kg h⁻¹, and the Secondary Clarifier ② as the least significant at 1.23 kg h⁻¹. The correlation coefficient R^2 for the measured and simulated concentrations is 0.63, with an RMSE of 0.70 mg m⁻³. On 13th December, the Aeration Tank ⑤ is the largest point source of CH4 emissions at 3.93 kg h⁻¹, and the Primary Clarifier ⑤ is the smallest at 0.55 kg h⁻¹, with a correlation

coefficient R^2 of 0.70 and an RMSE of 0.28 mg m^{-3}. The enhanced correlation between winter measurement and simulation data, as well as the improved fit of the measurement and simulation value curves, is attributed to the shorter monitoring cycle and more stable meteorological conditions.

In addition, when employing the multi-source Gaussian diffusion model combined with a genetic algorithm framework for iterative optimization to pinpoint point sources, we were able to locate external sources. As shown in Fig. S2 (a) and (c), external sources are primarily located along the main roadway to the south of the WWTP. Moreover, the estimated emissions vary across different days, which indicates that external source emissions are influenced by traffic vehicles. Fig. S2 (b) and (d) compare measured and simulated CH_4 concentrations before and after accounting for external sources, demonstrating that simulations are significantly closer to the measurements when external sources are included.
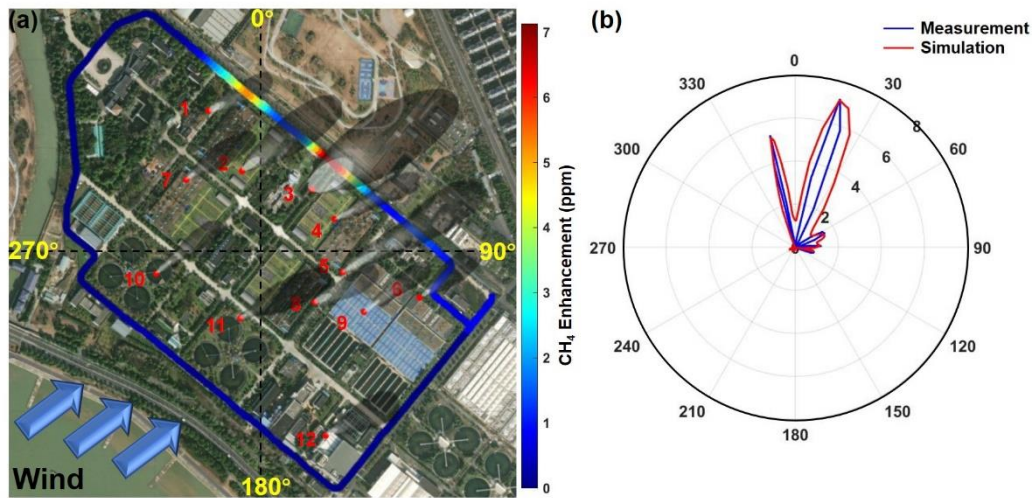
Figure 3. The emission distribution for the source locations (a) and the comparison between measured and simulated CH_4 concentrations (b) at the WWTP on 29th June. Map data are from ESRI.

389
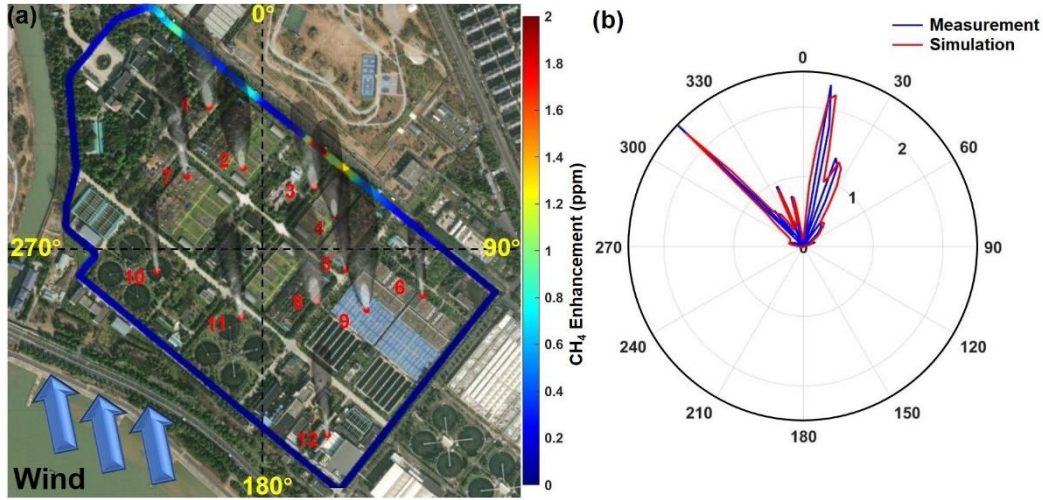
Figure 4. The emission distribution for the source locations (a) and the comparison between measured and simulated CH_4 concentrations (b) at the WWTP on 13th December. Map data are from ESRI.

Table 1 displays the CH_4 emission fluxes (Q), Wind speed and direction data (W_s, W_d), the horizontal diffusion coefficient (γ_1, α_1) and the vertical diffusion coefficient (γ_2, α_2) from the 8-day monitoring experiment. Wind speed and direction data are the average wind speed and direction during the monitoring time, and the CH_4 emission fluxes are obtained by the inversion of the average concentration, wind speed and direction data as input of the inversion framework. The emission flux values of CH_4 emission sources (12 point sources and 1 line source) for all experimental days are detailed in Tables S1 and S2. It is observed that the summer average CH_4 emission flux (68.78 ± 17.40 kg h^{-1}) surpasses the winter average CH_4 emission flux (47.76 ± 21.39 kg h^{-1}). This seasonal disparity in emissions is primarily attributed to the aeration tank, followed by the screen and primary clarifier. The activated sludge in the aeration tank contains a higher population of methanogens, whose CH_4 production capability intensifies with rising temperatures (Vítěz et al., 2020). Notably, the seasonal variance in the aeration tank is predominantly driven by the performance of the Aeration Tank ④. However, the substantial variation in the emissions from the three summer

experiments of the Aeration Tank ④ suggests a degree of emission instability. Conversely, the uniformity in the low emissions from the five winter experiments might be associated with the meteorological conditions and the actual operational status of the plant on those days. At lower wind speeds, the CH_4 emissions show only slight differences when compared to emissions on days with higher wind speeds. This suggests that the inversion results are less influenced by wind speed and are primarily associated with seasonal variations.

The screen and primary clarifier are the predominant emission sources at the WWTP. Specifically, these sources emit 37.50 kg h^{-1} in the summer and 31.92 kg h^{-1} in the winter, accounting for 55 % and 67 % of the total emissions. Pipeline leaks near the screen and primary clarifier lead to the CH_4 release. Previous research has similarly examined major emission sources at WWTPs. Yin et al. (2024) conducted offline monitoring of WWTPs in Beijing and Guiyang, identifying the primary treatment zone as the primary source of CH_4, accounting for 60.1 % and 35.8 % of the respective total emissions. Masuda et al. (2017) analyzed CH_4 emissions from different processes at three WWTPs in Japan, concluding that primary clarifiers are one of the major sources of CH_4 emissions. He et al. (2023) compiled CH_4 emission proportions for different processes in WWTPs based on reported data, finding percentages of 7 %-12 % for grit chamber, 8.2 %-68.1 % for primary clarifier, and 18.3 %-86.4 % for aeration tank.

Table 1. CH_4 emission fluxes (Q), Wind speed and direction data (W_s, W_d), the horizontal diffusion coefficient (γ_1, α_1) and the vertical diffusion coefficient (γ_2, α_2) from the 8-day monitoring experiment.

Date	Q (kg h^{-1})	W_s (m s^{-1})	W_d (°)	γ_1	α_1	γ_2	α_2
0601	61.85 ± 20.41	2.3	248.5	0.28	0.91	0.13	0.94
0629	74.92 ± 35.21	1.9	238.3	0.28	0.91	0.13	0.94
0711	69.58 ± 32.70	0.9	225.8	0.28	0.91	0.13	0.94

1213	49.19 ± 21.15	1.6	175.7	0.28	0.91	0.13	0.94
1214	43.29 ± 27.28	1.2	209.9	0.28	0.91	0.13	0.94
1220	49.99 ± 25.00	3.8	342.3	0.18	0.92	0.11	0.92
1221	48.17 ± 17.34	2.7	342.6	0.43	1.10	0.08	1.12
1222	48.15 ± 21.67	3.0	342.5	0.43	1.10	0.08	1.12

An alternative top-down approach known as the tracer gas dispersion method (TDM), which has been applied to estimate CH_4 emissions from city streets (von Fischer et al., 2017; Weller et al., 2018), WWTPs (Yoshida et al., 2014; Delre et al., 2017; Delre et al., 2018), biogas plants (Reinelt et al., 2017; Scheutz et al., 2019; Fredenslund et al., 2023) and landfills (Rees-White et al., 2019; Kissas et al., 2022). TDM involves releasing tracer gases like nitrous oxide and acetylene near the source and measuring their concentrations along with CH_4 downwind using a mobile platform. The similar diffusion patterns of CH_4 and the tracer gases result in a stable concentration ratio after atmospheric mixing, enabling the calculation of CH_4 emission rates with a better accuracy (Mønster et al., 2014).

Moreover, the TDM was employed to validate and compare other model inversion methods. Moore et al. (2023) proposed that the Gaussian dispersion modeling demands less experimental equipment, site access, and manpower than the TMD, which allows for swifter data gathering. Yacovitch et al. (2015) utilized a five-day dataset of tracer gas release in the Barnett shale region to evaluate the Gaussian dispersion flux quantification method. The results indicated a 95 % confidence interval, with a lower bound factor of 0.334 and an upper bound factor of 3.34. von Fischer et al. (2017) performed three controlled release experiments to validate the reliability of leak rate algorithm in Fort Collins, CO, which indicated a very significant correlation between known and estimated leak rates ($p < 0.0001$, $r^2 = 0.43$). Compared to the method employed in the study, the TDM offers advantages such as simpler formula calculations. Nonetheless, it also presents several drawbacks, including complex experimental

455 procedures, safety hazards associated with the release of tracer gases, which require

456 access permits from industrial facilities.

457 **3.3 Comparison with IPCC method**

458 The CH_4 emissions were also calculated using the IPCC method, with data sourced

459 from the Urban Drainage Statistical Yearbook of 2017. The emission flux of $213.95 \pm$

460 128.37 t a^{-1} was determined, with the uncertainty (60 %) derived from the data

461 summarized in the research (Lin et al., 2021). Figure 5 shows the contrast between the

462 emission inversion results from the monitoring experiment and the emission inventory.

463 The uncertainty of the inversion results was determined by accounting for the

464 uncertainties in wind speed, wind direction, and instrument measurements, following

465 the method presented in Section 2.4.5. The uncertainties in emission fluxes inversion

466 ranged from 33 % to 63 % on individual days. Notably, the uncertainty associated with

467 wind speed contributes approximately 44 % to 94 % of the uncertainty range. The

468 summer average inversion emission flux (603.33 ± 152.66 t a^{-1}) was calculated to be

469 2.8 times that of the inventory, and the winter average (418.95 ± 187.59 t a^{-1}) was twice

470 as much. It is posited that the discrepancy may stem from significant uncertainties in

471 the emission factors associated with the WWTPs or the lack of updated activity level

472 data, as the statistical yearbook provided data only up to 2017, the emission inventory

473 might have underestimated the actual emissions.

474 Furthermore, other studies have also investigated the comparison between CH_4

475 emissions obtained from different measurement methods at WWTPs and IPCC

476 inventory estimates. The majority of these studies indicate that the measured

477 values exceed the inventory values. Wang et al. (2021) conducted a measurement-

478 based assessment of CH_4 emissions (46.58 t a^{-1}) in Wuhu City, revealing a 46.71 %

479 higher than those calculated using the IPCC method. Moore et al. (2023)

480 employed mobile monitoring to evaluate CH_4 emissions at 63 WWTPs across the

481 United States. Specifically, CH_4 emissions from centrally treated domestic wastewater

in the U.S. amount to 4.64×10^5 t a^{-1}, which is 1.9 times greater than the EPA inventory. Song et al. (2023) investigated CH$_4$ emissions from municipal wastewater treatment in the U.S at $(4.36 \pm 2.8) \times 10^5$ t a^{-1}. This value was approximately twice the estimates provided by the IPCC. Our estimated results are generally consistent with the previous studies. The lower estimated results provided by the IPCC method can be attributed to the neglect of certain potential emission sources from the emission inventories, including emissions from equipment in sludge treatment facilities and leaks from pressure relief valves.
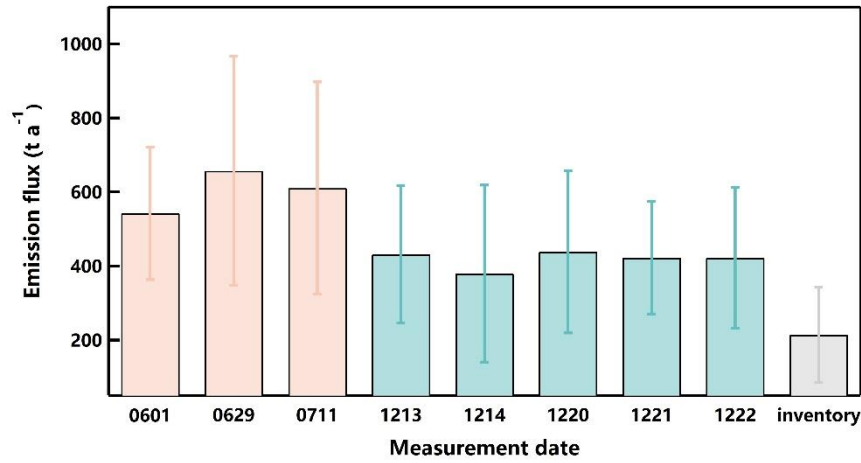
Figure 5. Comparison of CH$_4$ emission fluxes from the monitoring experiment and emission inventory in the WWTP.

3.4 Sensitivity analysis

In this section, we evaluated the stability of the inversion framework through sensitivity analysis and explored the impact of different point source locations on the inversion of emission concentrations. The precise identification of emission sources can enhance the accuracy of emission flux inversion, making a sensitivity analysis of the source location essential. We applied the method of controlling variables to perform a sensitivity analysis on the location of a single point source. The central position of the plant was taken as the reference origin, the positions of 12 emission sources were

502 determined to analyze the variation in error between measured and simulated

503 concentrations within a 200 m × 200 m range around each emission source. We

504 sequentially modified the source position parameters in the model input to analyze the

505 congruence between the simulated concentrations and the observed measurements,

506 quantifying the fit with RMSE. The change in concentration error serves as an indicator

507 of the accuracy of the emission source localization.

508   Figures 6 and 7 describe the error variation between monitored and simulated

509 concentrations when the point source location is subject to change within a 200 m ×

510 200 m range from the monitoring experiment on 29th June and 13th December. The error

511 variation of the remaining days can be seen in Figures S9-S14. The point source

512 locations simulated based on the inversion framework are mostly in areas with minor

513 relative concentration errors, which can be considered to have a high reliability in

514 simulating point source locations. The emission source location errors for the two

515 experiments are within the ranges of 0.7-1.3 mg m^{-3} and 0.2-0.3 mg m^{-3}. The winter

516 emission source locations exhibit greater stability and accuracy in the inversion results

517 than the summer ones.

518
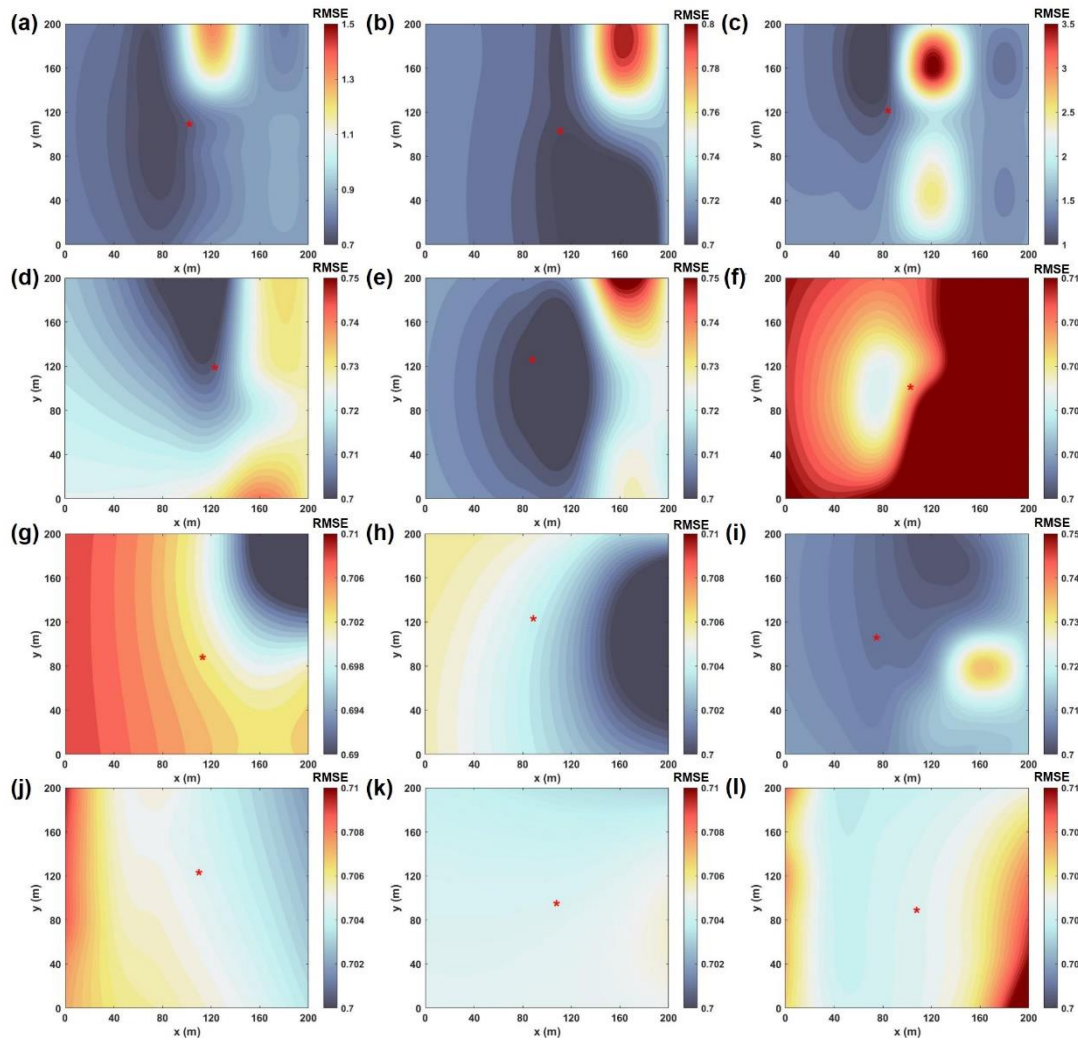
Figure 6. RMSE of monitoring simulated concentration changes with the location of WWTP source on 29th June. The x and y axes denote the horizontal and vertical distances of the simulated point source from the central point of the WWTP. The variation in color signifies the alteration in the root mean square error between the actual monitored and simulated concentrations, with the red star symbolizing the simulated point source location.
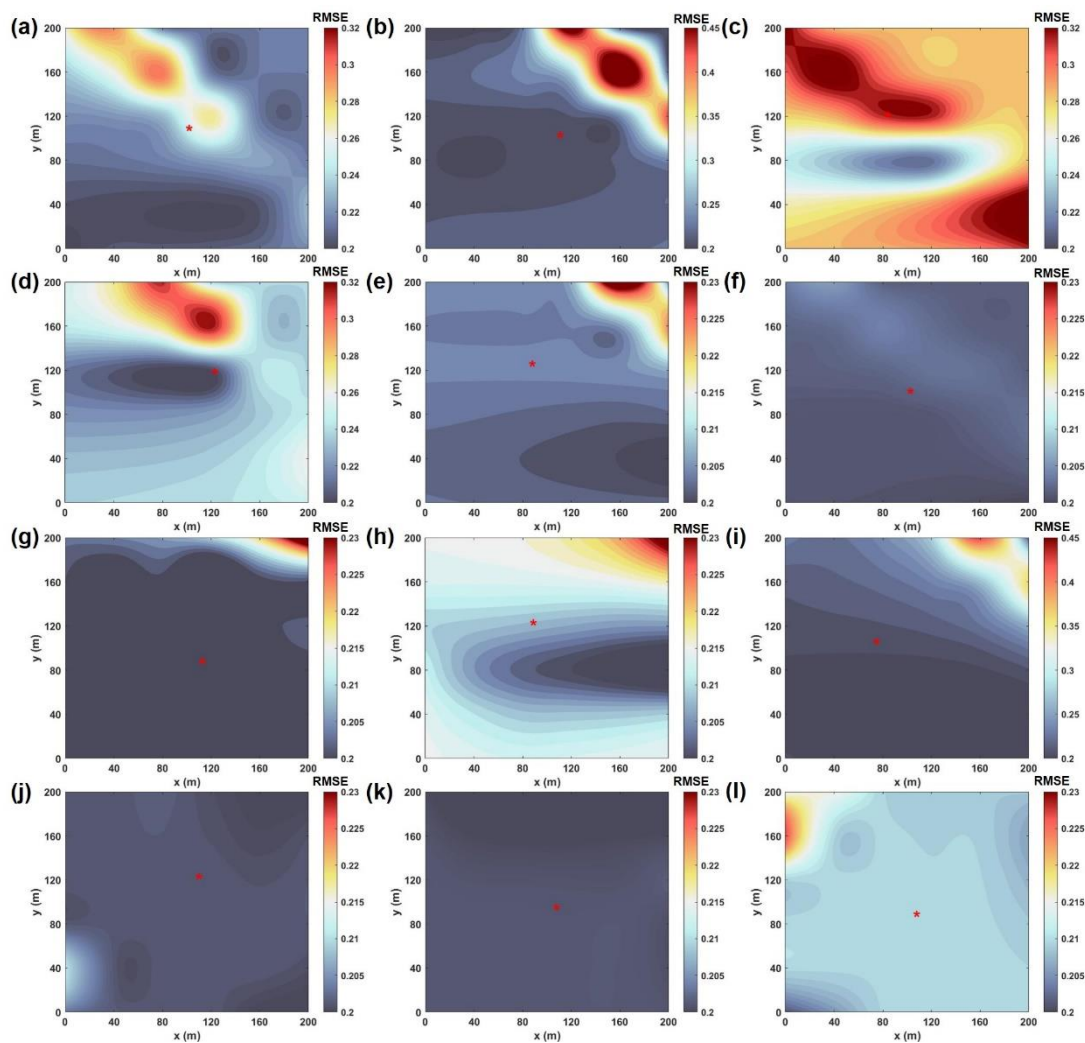
Figure 7. RMSE of monitoring simulated concentration changes with the location of WWTP source on 13th December.

4 Conclusions and outlook

The study carried out mobile measurements at a WWTP across the summer and winter seasons from Hangzhou 2023. By employing a multi-source Gaussian plume model combined with the genetic algorithm inversion framework, the inversion of CH_4 emission fluxes and their source locations was achieved. The results showed that 12 distinct CH_4 emission sources were pinpointed. The average CH_4 emission flux during the summer was 68.78 ± 17.40 kg h^{-1} (603.33 ± 152.66 t a^{-1}), and 47.76 ± 21.39 kg h^{-1} (418.95 ± 187.59 t a^{-1}) for the winter. The screen and primary clarifier were the main

sources, accounting for 55 % of summer and 67 % of winter emissions. The summer CH_4 inversion emissions were found to be 2.8 times higher, and the winter inversion emissions were twice as much as the inventory-based estimation.

The inversion framework is capable of validating emission coefficients in the inventory, identifying emission sources within the plant, and monitoring abnormal emissions. It can be applied to various monitoring systems, such as UAV systems and networks of fixed monitoring stations. We believe that it is an excellent point that collaborative monitoring offers significant improvements in the accuracy of emission fluxes and source inversion. Future efforts should aim to refine the inversion framework for broader applicability to various pollutant gases, enhancing the inversion efficiency, and extending the validation of the framework through monitoring experiments in a diverse range of industrial facilities.

Data availability. The raw data in this paper can be obtained from the corresponding author upon request.

Author contributions. ZW and YZ administrated the project and determined the main goal of this study. ZX, JY and XP designed the methods and planned the campaign. JY, ZX, YY, SZ and BQ performed the measurements. JY wrote the paper with contributions from all co-authors.

Competing interests. At least one of the (co-)authors is a member of the editorial board of Atmospheric Chemistry and Physics.

Financial support. The study has been supported by the National Key Research and Development Program of China (grant nos. 2022YFC3703500 and 2022YFE0209100), the National Natural Science Foundation of China (grant no. 42307129), the Key Research and Development Program of Zhejiang Province (grant nos. 2021C03165 and 2022C03084), the Zhejiang Provincial Natural Science Foundation (grant no. LZJMZ24D050005), and the Ecological Environment Research and Achievement Promotion Project of Zhejiang Province (grant nos. 2024XM0053 and 2024XM0052).

References

Abeywickrama, H. G. K., Bajón-Fernández, Y., Srinamasivayam, B., Turner, D., and Rivas Casado, M.: Development of a UAV based framework for CH_4 monitoring in sludge treatment centres, Remote Sens., 15, 3704, https://doi.org/10.3390/rs15153704, 2023.

Albertson, J. D., Harvey, T., Foderaro, G., Zhu, P., Zhou, X., Ferrari, S., Amin, M. S., Modrak, M., Brantley, H., and Thoma, E. D.: A Mobile Sensing Approach for regional surveillance of fugitive methane emissions in oil and gas production, Environ. Sci. Technol., 50, 2487-2497, https://doi.org/10.1021/acs.est.5b05059, 2016.

Allen, G., Hollingsworth, P., Kabbabe, K., Pitt, J. R., Mead, M. I., Illingworth, S., Roberts, G., Bourn, M., Shallcross, D. E., and Percival, C. J.: The development and trial of an unmanned aerial system for the measurement of methane flux from landfill and greenhouse gas emission hotspots, Waste Manage., 87, 883-892, https://doi.org/10.1016/j.wasman.2017.12.024, 2019.

Al-Shalan, A., Lowry, D., Fisher, R. E., Nisbet, E. G., Zazzeri, G., Al-Sarawi, M., France, J. L.: Methane emissions in Kuwait: Plume identification, isotopic characterisation and inventory verification, Atmos. Environ., 268, 118763, https://doi.org/10.1016/j.atmosenv.2021.118763, 2022.

Alshboul, Z., Encinas-Fernández, J., Hofmann, H., and Lorke, A.: Export of dissolved methane and carbon dioxide with effluents from municipal wastewater treatment plants, Environ. Sci. Technol., 50, 5555-5563, https://doi.org/10.1021/acs.est.5b04923, 2016.

Bai, R. L., Jin, L., Sun, S. R., Cheng, Y., and Wei, Y.: Quantification of greenhouse gas emission from wastewater treatment plants, Greenhouse. Gas. Sci. Technol., 12, 587-601, https://doi.org/10.1002/ghg.2171, 2022.

Balashov, N. V., Davis, K. J., Miles, N. L., Lauvaux, T., Richardson, S. J., Barkley, Z.

R., and Bonin, T. A.: Background heterogeneity and other uncertainties in estimating urban methane flux: results from the Indianapolis Flux Experiment (INFLUX), Atmos. Chem. Phys., 20, 4545-4559, https://doi.org/10.5194/acp-20-4545-2020, 2020.

Bao, Z., Sun, S., and Sun, D.: Assessment of greenhouse gas emission from A/O and SBR wastewater treatment plants in Beijing, China. Int. Biodeterior. Biodegrad., 108, 108-114, https://doi.org/10.1016/j.ibiod.2015.11.028, 2016.

Bergamaschi, P., Karstens, U., Manning, A. J., Saunois, M., Tsuruta, A., Berchet, A., Vermeulen, A. T., Arnold, T., Janssens-Maenhout, G., Hammer, S., Levin, I., Schmidt, M., Ramonet, M., Lopez, M., Lavric, J., Aalto, T., Chen, H., Feist, D. G., Gerbig, C., Haszpra, L., Hermansen, O., Manca, G., Moncrieff, J., Meinhardt, F., Necki, J., Galkowski, M., O'Doherty, S., Paramonova, N., Scheeren, H. A., Steinbacher, M., and Dlugokencky, E.: Inverse modelling of European CH_4 emissions during 2006-2012 using different inverse models and reassessed atmospheric observations, Atmos. Chem. Phys., 18, 901-920, https://doi.org/10.5194/acp-18-901-2018, 2018.

Cai, B., Gao, Q., Li, Z., Wu, J., Cao, D., and Liu, L.: Study on the methane emission factors of wastewater treatment plants in China, China Population Resources and Environment, 25, 118-124, https://doi.org/10.3969/j.issn.1002-2104.2015.04.015, 2015.

Caulton, D. R., Li, Q., Bou-Zeid, E., Fitts, J. P., Golston, L. M., Pan, D., Lu, J., Lane, H. M., Buchholz, B., Guo, X., McSpiritt, J., Wendt, L., and Zondlo, M. A.: Quantifying uncertainties from mobile-laboratory-derived emissions of well pads using inverse Gaussian methods, Atmos. Chem. Phys., 18, 15145-15168, https://doi.org/10.5194/acp-18-15145-2018, 2018.

Chen, J., Dietrich, F., Maazallahi, H., Forstmaier, A., Winkler, D., Hofmann, M. E. G., Denier van der Gon, H., and Röckmann, T.: Methane emissions from the Munich Oktoberfest, Atmos. Chem. Phys., 20, 3683-3696, https://doi.org/10.5194/acp-20-3683-2020, 2020.

Cui, Y. Y., Brioude, J., Angevine, W. M., Peischl, J., McKeen, S. A., Kim, S.-W., Neuman, J. A., Henze, D. K., Bousserez, N., Fischer, M. L., Jeong, S., Michelsen, H. A., Bambha, R. P., Liu, Z., Santoni, G. W., Daube, B. C., Kort, E. A., Frost, G. J., Ryerson, T., Wofsy, S. C., and Trainer, M.: Top-down estimate of methane emissions in California using a mesoscale inverse modeling technique: The San Joaquin Valley, J. Geophys. Res., 122, 3686-3699, https://doi.org/10.1002/2016JD026398, 2017.

Cusworth, D. H., Duren, R. M., Ayasse, A. K., Jiorle, R., Howell, K., Aubrey, A., Green, R. O., Eastwood, M. L., Chapman, J. W., Thorpe, A. K., Heckler, J., Asner, G. P., Smith, M. L., Thoma, E., Krause, M. J., Heins, D., and Thorneloe, S.: Quantifying methane emissions from United States landfills, Science, 383, 1499-1504, https://www.science.org/doi/10.1126/science.adi7735, 2024.

Defratyka, S. M., Paris, J. D., Yver-Kwok, C., Fernandez, J. M., Korben, P., and Bousquet, P.: Mapping urban methane sources in Paris, France, Environ. Sci. Technol., 55, 8583-8591, https://doi.org/10.1021/acs.est.1c00859, 2021.

Delre, A., Mønster, J., and Scheutz, C.: Greenhouse gas emission quantification from wastewater treatment plants, using a tracer gas dispersion method, Sci. Total. Environ., 605-606, 258-268, http://dx.doi.org/10.1016/j.scitotenv.2017.06.177, 2017.

Delre, A., Mønster, J., Samuelsson, J., Fredenslund, A. M., and Scheutz, C.: Emission quantification using the tracer gas dispersion method: the influence of instrument, tracer gas species and source simulation, Sci. Total. Environ., 634, 59-66, https://doi.org/10.1016/j.scitotenv.2018.03.289, 2018.

Dietrich, F., Chen, J., Voggenreiter, B., Aigner, P., Nachtigall, N., and Reger, B.: MUCCnet: Munich Urban Carbon Column network, Atmos. Meas. Tech., 14, 1111-1126, https://doi.org/10.5194/amt-14-1111-2021, 2021.

Fredenslund, A. M., Gudmundsson, E., Falk, J. M., and Scheutz, C.: The Danish national effort to minimise methane emissions from biogas plants, Waste Manage., 157, 321-329, https://doi.org/10.1016/j.wasman.2022.12.035, 2023.

Guisasola, A., de Haas, D., Keller, J., and Yuan, Z.: Methane formation in sewer systems.

Water Res., 42, 1421-1430, https://doi.org/10.1016/j.watres.2007.10.014, 2008.

Guo, S., Huang, H., Dong, X., and Zeng, S.: Calculation of greenhouse gas emissions of municipal wastewater treatment and its temporal and spatial trend in China, Water &Wastewater Engineering, 45, 56-62, https://doi.org/10.13789/j.cnki.wwe1964.2019.04.009, 2019.

Hase, F., Frey, M., Blumenstock, T., Groß, J., Kiel, M., Kohlhepp, R., Mengistu Tsidu, G., Schäfer, K., Sha, M. K., and Orphal, J.: Application of portable FTIR spectrometers for detecting greenhouse gas emissions of the major city Berlin, Atmos. Meas. Tech., 8, 3059-3068, https://doi.org/10.5194/amt-8-3059-2015, 2015.

Han, G., Pei, Z., Shi, T., Mao, H., Li, S., Mao, F., Ma, X., Zhang, X., and Gong, W.: Unveiling unprecedented methane hotspots in China's leading coal production hub: a satellite mapping revelation, Geophys. Res. Lett., 51, e2024GL109065, https://doi.org/10.1029/2024GL109065, 2024.

Heerah, S., Frausto-Vicencio, I., Jeong, S., Marklein, A. R., Ding, Y., Meyer, A. G., Parker, H. A., Fischer, M. L., Franklin, J. E., Hopkins, F. M., and Dubey, M.: Dairy methane emissions in California's San Joaquin Valley inferred with ground-based remote sensing observations in the summer and winter, J. Geophys. Res-Atmos., 126, e2021JD034785, https://doi.org/10.1029/2021JD03478, 2021.

Harada, T., and Alba, E.: Parallel genetic algorithms: a useful survey, ACM Comput. Surv., 53, 1-39, https://doi.org/10.1145/3400031, 2020.

He, Y., Li, Y., Li, X., Liu, Y., Wang, Y., Guo, H., Hou, J., Zhu, T., and Liu, Y.: Net-zero greenhouse gas emission from wastewater treatment: mechanisms, opportunities and perspectives, Renew. Sust. Energ. Rev., 184, 113547, https://doi.org/10.1016/j.rser.2023.113547, 2023.

IPCC: Climate Change 2023: Synthesis Report. Contribution of Working Groups I, II and III to the Sixth Assessment Report of the Intergovernmental Panel on Climate Change, 35-115, https://doi.org/10.59327/IPCC/AR6-9789291691647, 2023.

Jackson, R. B., Down, A., Phillips, N. G., Ackley, R. C., Cook, C. W., Plata, D. L., and

Zhao, K.: Natural gas pipeline leaks across Washington, DC, Environ. Sci. Technol., 48, 2051-2058, https://doi.org/10.1021/es404474x, 2014.

Jacob, D. J., Varon, D. J., Cusworth, D. H., Dennison, P. E., Frankenberg, C., Gautam, R., Guanter, L., Kelley, J., McKeever, J., Ott, L. E., Poulter, B., Qu, Z., Thorpe, A. K., Worden, J. R., and Duren, R. M.: Quantifying methane emissions from the global scale down to point sources using satellite observations of atmospheric methane, Atmos. Chem. Phys., 22, 9617-9646, https://doi.org/10.5194/acp-22-9617-2022, 2022.

Karion, A., Lauvaux, T., Lopez Coto, I., Sweeney, C., Mueller, K., Gourdji, S., Angevine, W., Barkley, Z., Deng, A., Andrews, A., Stein, A., and Whetstone, J.: Intercomparison of atmospheric trace gas dispersion models: Barnett Shale case study, Atmos. Chem. Phys., 19, 2561-2576, https://doi.org/10.5194/acp-19-2561-2019, 2019.

Katoch, S., Chauhan, S.S. and Kumar, V.: A review on genetic algorithm: past, present, and future. Multimed. Tools Appl., 80, 8091-8126, https://doi.org/10.1007/s11042-020-10139-6, 2021.

Kissas, K., Ibrom, A., Kjeldsen, P., and Scheutz, C.: Methane emission dynamics from a Danish landfill: The effect of changes in barometric pressure, Waste Manage., 138, 234-242, https://doi.org/10.1016/j.wasman.2021.11.043, 2022.

Kumar, P., Broquet, G., Yver-Kwok, C., Laurent, O., Gichuki, S., Caldow, C., Cropley, F., Lauvaux, T., Ramonet, M., Berthe, G., Martin, F., Duclaux, O., Juery, C., Bouchet, C., and Ciais, P.: Mobile atmospheric measurements and local-scale inverse estimation of the location and rates of brief CH_4 and CO_2 releases from point sources, Atmos. Meas. Tech., 14, 5987-6003, https://doi.org/10.5194/amt-14-5987-2021, 2021.

Li, H., You, L., Du, H., Yu, B., Lu, L., Zheng, B., Zhang, Q., He, K., and Ren, N.: Methane and nitrous oxide emissions from municipal wastewater treatment plants in China: a plant-level and technology-specific study, Environ. Sci. Technol., 20,

100345, https://doi.org/10.1016/j.ese.2023.100345, 2024.

Liang, R., Zhang, Y., Chen, W., Zhang, P., Liu, J., Chen, C., Mao, H., Shen, G., Qu, Z., Chen, Z., Zhou, M., Wang, P., Parker, R. J., Boesch, H., Lorente, A., Maasakkers, J.D., and Aben, I.: East Asian methane emissions inferred from high-resolution inversions of GOSAT and TROPOMI observations: a comparative and evaluative analysis, Atmos. Chem. Phys., 23, 8039-8057, https://doi.org/10.5194/acp-23-8039-2023, 2023.

Lin, X., Zhang, W., Crippa, M., Peng, S., Han, P., Zeng, N., Yu, L., and Wang, G.: A comparative study of anthropogenic CH_4 emissions over China based on the ensembles of bottom-up inventories, Earth Syst. Sci. Data, 13, 1073-1088, https://doi.org/10.5194/essd-13-1073-2021, 2021.

Lopez, M., Sherwood, O. A., Dlugokencky, E. J., Kessler, R., Giroux, L., and Worthy, D. E. J.: Isotopic signatures of anthropogenic CH_4 sources in Alberta, Canada, Atmos. Environ., 164, 280-288, https://doi.org/10.1016/j.atmosenv.2017.06.021, 2017.

Luther, A., Kleinschek, R., Scheidweiler, L., Defratyka, S., Stanisavljevic, M., Forstmaier, A., Dandocsi, A., Wolff, S., Dubravica, D., Wildmann, N., Kostinek, J., Jöckel, P., Nickl, A.-L., Klausner, T., Hase, F., Frey, M., Chen, J., Dietrich, F., Nęcki, J., Swolkień, J., Fix, A., Roiger, A., and Butz, A.: Quantifying CH_4 emissions from hard coal mines using mobile sun-viewing Fourier transform spectrometry, Atmos. Meas. Tech., 12, 5217-5230, https://doi.org/10.5194/amt-12-5217-2019, 2019.

Maazallahi, H., Fernandez, J. M., Menoud, M., Zavala-Araiza, D., Weller, Z. D., Schwietzke, S., von Fischer, J. C., Denier van der Gon, H., and Röckmann, T.: Methane mapping, emission quantification, and attribution in two European cities: Utrecht (NL) and Hamburg (DE), Atmos. Chem. Phys., 20, 14717-14740, https://doi.org/10.5194/acp-20-14717-2020, 2020.

Maazallahi, H., Delre, A., Scheutz, C., Fredenslund, A. M., Schwietzke, S., Denier van der Gon, H., and Röckmann, T.: Intercomparison of detection and quantification methods for methane emissions from the natural gas distribution network in

Hamburg, Germany, Atmos. Meas. Tech., 16, 5051-5073, https://doi.org/10.5194/amt-16-5051-2023, 2023.

Makarova, M. V., Alberti, C., Ionov, D. V., Hase, F., Foka, S. C., Blumenstock, T., Warneke, T., Virolainen, Y. A., Kostsov, V. S., Frey, M., Poberovskii, A. V., Timofeyev, Y. M., Paramonova, N. N., Volkova, K. A., Zaitsev, N. A., Biryukov, E. Y., Osipov, S. I., Makarov, B. K., Polyakov, A. V., Ivakhov, V. M., Imhasin, H. K., and Mikhailov, E. F.: Emission Monitoring Mobile Experiment (EMME): an overview and first results of the St. Petersburg megacity campaign 2019, Atmos. Meas. Tech., 14, 1047-1073, https://doi.org/10.5194/amt-14-1047-2021, 2021.

Masuda, S., Suzuki, S., Sano, I., Li, Y.-Y., and Nishimura, O.: The seasonal variation of emission of greenhouse gases from a full-scale sewage treatment plant, Chemosphere, 140, 167-173, https://doi.org/10.1016/j.chemosphere.2014.09.042, 2015.

Masuda, S., Sano, I., Hojo, T., Li, Y.-Y., and Nishimura, O.: The comparison of greenhouse gas emissions in sewage treatment plants with different treatment processes, Chemosphere, 193, 581-590, https://doi.org/10.1016/j.chemosphere.2017.11.018, 2017.

McKain, K., Down, A., Raciti, S. M., Budney, J., Hutyra, L. R., Floerchinger, C., Herndon, S. C., Nehrkorn, T., Zahniser, M. S., Jackson, R. B., Phillips, N., and Wofsy, S. C.: Methane emissions from natural gas infrastructure and use in the urban region of Boston, Massachusetts, Proc. Natl. Acad. Sci. U.S.A., 112, 1941-1946, https://doi.org/10.1073/pnas.1416261112, 2015.

Mønster, J., Samuelsson, J., Kjeldsen, P., Rella, C.W., and Scheutz, C.: Quantifying methane emission from fugitive sources by combining tracer release and downwind measurements- A sensitivity analysis based on multiple field surveys, Waste Manage., 34, 1416-1428, https://doi.org/10.1016/j.wasman.2014.03.025, 2014.

Moore, D. P., Li, N. P., Wendt, L. P., Castañeda, S. R., Falinski, M. M., Zhu, J.-J., Song, C., Ren, Z. J., and Zondlo, M. A.: Underestimation of sector-wide methane emissions from united states wastewater treatment, Environ. Sci. Technol., 57, 4082-4090,

https://doi.org/10.1021/acs.est.2c05373, 2023.

Nassar, R., Hill, T. G., McLinden, C. A., Wunch, D., Jones, D. B. A., and Crisp, D.: Quantifying CO_2 emissions from individual power plants from Space, Geophys. Res. Let.t, 44, 10045-10053, https://doi.org/10.1002/2017GL074702, 2017.

Picarro: Datasheet G2201-i $\delta^{13}C$ in CH_4 and CO_2 Gas Analyzer, available at: https://www.picarro.com/environmental/support/library/documents/g2201i_analyzer_datasheet (last access: 5 August 2024), 2010.

Rees-White, T. C., Mønster, J., Beaven, R. P., and Scheutz, C.: Measuring methane emissions from a UK landfill using the tracer dispersion method and the influence of operational and environmental factors, Waste Manage., 87, 870-882, https://doi.org/10.1016/j.wasman.2018.03.023, 2019.

Reinelt, T., Delre, A., Westerkamp, T., Holmgren, M.A., Liebetrau, J., and Scheutz, C.: Comparative use of different emission measurement approaches to determine methane emissions from a biogas plant, Waste Manage., 68, 173-185, http://dx.doi.org/10.1016/j.wasman.2017.05.053, 2017.

Rella, C. W., Hoffnagle, J., He, Y., and Tajima, S.: Local- and regional-scale measurements of CH_4, $\delta^{13}CH_4$, and C_2H_6 in the Uintah Basin using a mobile stable isotope analyzer, Atmos. Meas. Tech., 8, 4539-4559, https://doi.org/10.5194/amt-8-4539-2015, 2015.

Richardson, S. J., Miles, N. L., Davis, K. J., Lauvaux, T., Martins, D. K., Turnbull, J. C., McKain, K., Sweeney, C., and Cambaliza, M. O. L.: Tower measurement network of in-situ CO_2, CH_4, and CO in support of the Indianapolis FLUX (INFLUX) Experiment, Elem. Sci. Anth., 5, 59, https://doi.org/10.1525/elementa.140, 2017.

Riddick, S. N., Connors, S., Robinson, A. D., Manning, A. J., Jones, P. S. D., Lowry, D., Nisbet, E., Skelton, R. L., Allen, G., Pitt, J., and Harris, N. R. P.: Estimating the size of a methane emission point source at different scales: from local to landscape, Atmos. Chem. Phys., 17, 7839-7851, https://doi.org/10.5194/acp-17-7839-2017, 2017.

Scheutz, C., and Kjeldsen, P.: Guidelines for landfill gas emission monitoring using the tracer gas dispersion method, Waste Manage., 85, 351-360, https://doi.org/10.1016/j.wasman.2018.12.048, 2019.

Shi, T., Han, G., Ma, X., Mao, H., Chen, C., Han, Z., Pei, Z., Zhang, H., Li, S., and Gong, W.: Quantifying factory-scale CO_2/CH_4 emission based on mobile measurements and EMISSION-PARTITION model: cases in China, Environ. Res. Lett., 18, 034028, https://doi.org/10.1088/1748-9326/acbce7, 2023.

Song, C., Zhu, J.-J., Willis, J. L., Moore, D. P., Zondlo, M. A., and Ren, Z. J.: Methane emissions from municipal wastewater collection and treatment systems, Environ. Sci. Technol., 57, 2248-2261, https://doi.org/10.1021/acs.est.2c04388, 2023.

Stadler, C., Fusé, V. S., Linares, S., and Juliarena, P.: Estimation of methane emission from an urban wastewater treatment plant applying inverse Gaussian model, Environ. Monit. Assess., 194, 27, https://doi.org/10.1007/s10661-021-09660-4, 2021.

Sun, W., Deng, L., Wu, G., Wu, L., Han, P., Miao, Y., and Yao, B.: Atmospheric monitoring of methane in Beijing using a mobile observatory, Atmosphere, 10, 554, https://doi.org/10.3390/atmos10090554, 2019.

Sun, Y., Yang, T., Gui, H., Li, X., Wang, W., Duan, J., Mao, S., Yin, H., Zhou, B., Lang, J., Zhou, H., Liu, C., and Xie, P.: Atmospheric environment monitoring technology and equipment in China: a review and outlook, J. Environ. Sci., 123, 41-53, https://doi.org/10.1016/j.jes.2022.01.014, 2023.

Venkatram, A. and Horst, T. W.: Approximating dispersion from a finite line source, Atmos. Environ., 40, 2401-2408, https://doi.org/10.1016/j.atmosenv.2005.12.014, 2006.

Vítěz, T., Novák, D., Lochman, J., and Vítězová, M.: Methanogens diversity during anaerobic sewage sludge stabilization and the effect of temperature, Processes, 8, 822, https://doi.org/10.3390/pr8070822, 2020.

Vogel, F., Ars, S., Wunch, D., Lavoie, J., Gillespie, L., Maazallahi, H., Röckmann, T., Nęcki, J., Bartyzel, J., Jagoda, P., Lowry, D., France, J., Fernandez, J., Bakkaloglu,

S., Fisher, R., Lanoiselle, M., Chen, H., Oudshoorn, M., Yver-Kwok, C., Defratyka, S., Morgui, J. A., Estruch, C., Curcoll, R., Grossi, C., Chen, J., Dietrich, F., Forstmaier, A., Denier van der Gon, H. A. C., Dellaert, S. N. C., Salo, J., Corbu, M., Iancu, S. S., Tudor, A. S., Scarlat, A. I., and Calcan, A.: Ground-based mobile measurements to track urban methane emissions from natural gas in 12 cities across eight countries, Environ. Sci. Technol., 58, 2271-2281, https://doi.org/10.1021/acs.est.3c03160, 2024.

von Fischer, J. C., Cooley, D., Chamberlain, S., Gaylord, A., Griebenow, C. J., Hamburg, S. P., Salo, J., Schumacher, R., Theobald, D., and Ham, J.: Rapid, vehicle-based identification of location and magnitude of urban natural gas pipeline leaks, Environ. Sci. Technol., 51, 4091-4099, https://doi.org/10.1021/acs.est.6b06095, 2017.

Wang, X., Wang, T., Chen, S., and Tang, Y.: Study on methane emission from wastewater treatment plants-A case study of Wuhu city, Advances in Geosciences, 11, 677-689, https://doi.org/10.12677/AG.2021.115063, 2021.

WMO:WMO greenhouse gas Bulletin. The state of greenhouse gases in the atmosphere based on global observations through 2022. https://library.wmo.int/idurl/4/68532, 2023.

Weller, Z. D., Roscioli, J. R., Daube, W. C., Lamb, B. K., Ferrara, T. W., Brewer, P. E., and von Fischer, J. C.: Vehicle-based methane surveys for finding natural gas leaks and estimating their size: validation and uncertainty, Environ. Sci. Technol., 52, 11922-11930, https://doi.org/10.1021/acs.est.8b03135, 2018.

Weller, Z. D., Yang, D.K., von Fischer, J.C.: An open source algorithm to detect natural gas leaks from mobile methane survey data, PLoS ONE, 14, e0212287, https://doi.org/10.1371/journal.pone.0212287, 2019.

Yacovitch, T. I., Herndon, S. C., Petron, G., Kofler, J., Lyon, D., Zahniser, M. S., and Kolb, C. E.: Mobile laboratory observations of methane emissions in the Barnett Shale Region, Environ. Sci. Technol., 49, 7889-7895, https://doi.org/10.1021/es506352j, 2015.

Yin, Y., Qi, X., Gao, L., Lu, X., Yang, X., Xiao, K., Liu, Y., Qiu, Y., Huang, X., and Liang, P.: Quantifying methane influx from sewer into wastewater treatment processes, Environ. Sci. Technol., 58, 9582-9590, https://doi.org/10.1021/acs.est.4c00820, 2024.

Yoshida, H., Mønster, J., and Scheutz, C.: Plant-integrated measurement of greenhouse gas emissions from a municipal wastewater treatment plant, Water Res., 61, 108-118, http://dx.doi.org/10.1016/j.watres.2014.05.014, 2014.

Zhang, Y., Jacob, D. J., Lu, X., Maasakkers, J. D., Scarpelli, T. R., Sheng, J.-X., Shen, L., Qu, Z., Sulprizio, M. P., Chang, J., Bloom, A. A., Ma, S., Worden, J., Parker, R. J., and Boesch, H.: Attribution of the accelerating increase in atmospheric methane during 2010-2018 by inverse analysis of GOSAT observations, Atmos. Chem. Phys., 21, 3643-3666, https://doi.org/10.5194/acp-21-3643-2021, 2021.

Zhao, S., Zhang, Y., Liang, R., Chen, W., Xie, X., Wang, R., Xia, Z., Shen, J., Wang, Y., and Chen, H.: Low methane emissions from the natural gas distribution system indicated by mobile measurements in a Chinese megacity Hangzhou, Environ. Sci. Technol. Air, 1, 1511-1518, https://doi.org/10.1021/acsestair.4c00068, 2024.

Zhao, T., Yang, D., Liu, Y., Cai, Z., Yao, L., Che, K., Ren, X., Bi, Y., Yi, Y., Wang, J., and Zhu, S.: Development of an integrated lightweight multi-rotor UAV payload for atmospheric carbon dioxide mole fraction measurements, Atmosphere, 13, 855, https://doi.org/10.3390/atmos13060855, 2022.

Zhao, Y., Xue, M., Li, X., Liu, G., Liu, S., and Sun, X.: Application of vehicle-mounted methane detection method in the oil and gas industry, Environmental Protection of Oil & Gas Fields, 31, 4, https://doi.org/10.3969/j.issn.1005-3158.2021.04.001, 2021.

Zimnoch, M., Necki, J., Chmura, L., Jasek, A., Jelen, D., Galkowski, M., Kuc, T., Gorczyca, Z., Bartyzel, J., and Rozanski, K.: Quantification of carbon dioxide and methane emissions in urban areas: source apportionment based on atmospheric observations, Mitig. Adapt. Strateg. Glob. Change, 24, 1051-1071, https://doi.org/10.1007/s11027-018-9821-0, 2018.